NOTCH Activation Promotes Valve Formation by Regulating the Endocardial Secretome

Authors

Rebeca Torregrosa-Carrión, Luis Luna-Zurita, Fernando García-Marqués, Gaetano D'Amato, Rebeca Piñeiro-Sabarís, Elena Bonzón-Kulichenko, Jesús Vázquez, and José Luis de la Pompa

Correspondence

jlpompa@cnic.es

In Brief

The NOTCH-dependent endocardial secretome has been determined by quantitative MS-based proteomics of mouse embryonic endocardial cells (MEEC). DLL4-mediated NOTCH activation lead to expression of EMT, cytoskeleton and cell-cell/cell-matrix proteins, whereas JAG1-NOTCH signaling activated ECM molecules expression. Data validation *in vitro* and *in vivo* support the value of MEEC as a model for studying the endocardial secretome and for the identification of novel factors potentially involved in heart development and disease.

Graphical Abstract
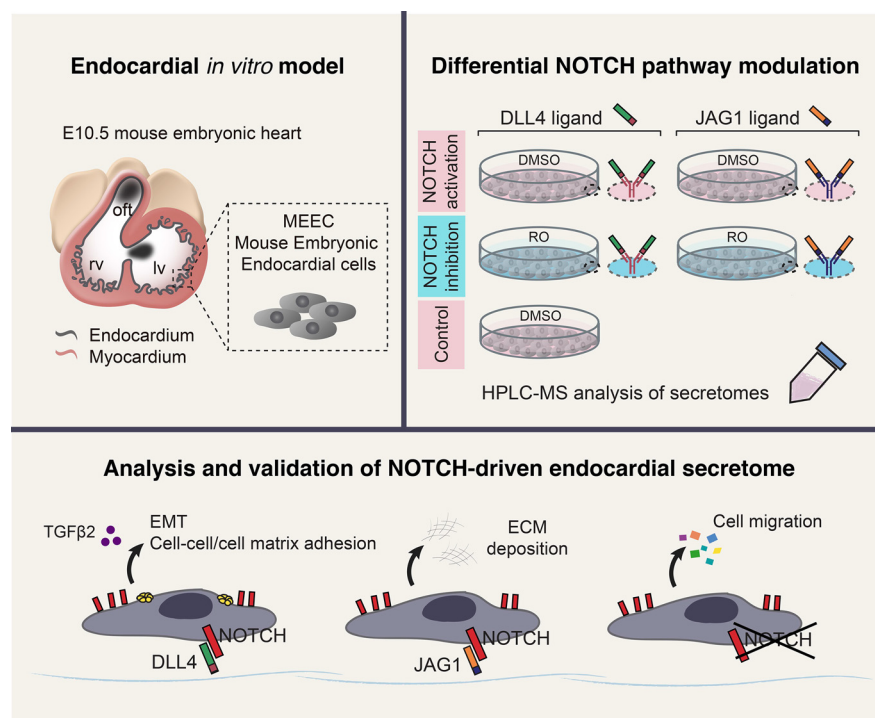
Highlights

- MEEC are a reliable endocardial *in vitro* model.

- Quantitative proteomics to characterize the NOTCH-driven endocardial secretome.

- NOTCH pathway status underlies different paracrine biological functions.

- New insights into secreted factors involved in cardiac valve development.

NOTCH Activation Promotes Valve Formation by Regulating the Endocardial Secretome*⑤

Rebeca Torregrosa-Carrión‡§, Luis Luna-Zurita‡§, ⬤ Fernando García-Marqués¶, Gaetano D'Amato‡‖, Rebeca Piñeiro-Sabarís‡§, Elena Bonzón-Kulichenko§, Jesús Vázquez§**, and ⬤ José Luis de la Pompa‡§‡‡**

The endocardium is a specialized endothelium that lines the inner surface of the heart. Functional studies in mice and zebrafish have established that the endocardium is a source of instructive signals for the development of cardiac structures, including the heart valves and chambers. Here, we characterized the NOTCH-dependent endocardial secretome by manipulating NOTCH activity in mouse embryonic endocardial cells (MEEC) followed by mass spectrometry-based proteomics. We profiled different sets of soluble factors whose secretion not only responds to NOTCH activation but also shows differential ligand specificity, suggesting that ligand-specific inputs may regulate the expression of secreted proteins involved in different cardiac development processes. NOTCH signaling activation correlates with a transforming growth factor-β2 (TGFβ2)-rich secretome and the delivery of paracrine signals involved in focal adhesion and extracellular matrix (ECM) deposition and remodeling. In contrast, NOTCH inhibition is accompanied by the up-regulation of specific semaphorins that may modulate cell migration. The secretome protein expression data showed a good correlation with gene profiling of RNA expression in embryonic endocardial cells. Additional characterization by *in situ* hybridization in mouse embryos revealed expression of various NOTCH candidate effector genes (*Tgfβ2, Loxl2, Ptx3, Timp3, Fbln2*, and *Dc*n) in heart valve endocardium and/or mesenchyme. Validating these results, mice with conditional *Dll4* or *Jag1* loss-of-function mutations showed gene expression alterations similar to those observed at the protein level *in vitro*. These results provide the first description of the NOTCH-dependent endocardial secretome and validate MEEC as a tool for assaying the endocardial secretome response to a variety of stimuli and the potential use of this system for drug screening. *Molecular & Cellular Proteomics 18: 1782–1795, 2019. DOI: 10.1074/mcp.RA119.001492.*

Signaling interactions are crucial during the various stages of vertebrate cardiac development, from heart mesoderm specification and migration through heart tube formation and looping to the development, morphogenesis, and maturation of the heart valves and chambers. The early heart tube is formed by an outer epithelial myocardium and an inner endocardial layer separated by an extracellular matrix, the cardiac jelly. Inductive signaling between these two cell layers is crucial for the development of specialized heart structures, such as the valves and chambers.

During the formation of the heart valves, myocardium-derived BMP2 (1, 2) and endocardium-derived NOTCH signals (3), active in the prospective valve territory of the atrio-ventricular canal (AVC) region, function in concert to induce the epithelial-mesenchyme transition (EMT) of AVC endocardial cells (4, 5). Transformed mesenchyme cells lose cell-cell junctions, migrate, and colonize the AVC cardiac jelly to form the endocardial cushions, which will later protrude into the heart tube and function as primitive heart valves. Later, these mesenchymal cells proliferate and remodel by condensation and elongation, to give rise to the delicate valve leaflets and septum of the mature heart (6).

NOTCH is a conserved family of single-pass transmembrane receptors that are activated by membrane-bound ligands of the DELTA (DLL1, DLL3, and DLL4) and JAGGED/SERRATE (JAG1 and JAG2) families. Ligand-receptor interaction leads to a series of proteolytic processing events in the receptor that ultimately result in the generation of the NOTCH intracellular domain, which translocate to the cell nucleus and binds to a preexisting transcriptional complex to regulate target gene expression (7). The many roles of NOTCH in mammalian heart development include cardiac fate specification (8), heart tube patterning, and morphogenesis of cardiac structures; moreover, NOTCH signaling alterations leads to cardiac disease in humans (9). A key feature of NOTCH function in the heart is that it exerts non-cell autonomous effects on neighboring tissues. This is exemplified by the effect of endocardial NOTCH activity on myocardial pattern-

ing, presumably because NOTCH is required for the production of endocardial signals acting on the myocardium (4, 10–13). Candidate signaling molecules have been identified by gene expression profiling of NOTCH loss- or gain-of-function models (4, 10, 12, 13), but so far, there has been a lack of experimental models suitable for the proteomic identification of secreted endocardial proteins involved in cardiac development.

Here, we used mouse embryonic endocardial cells (MEEC) as an *in vitro* system to identify the NOTCH-dependent embryonic endocardial secretome. MEEC were stimulated with recombinant DLL4 and JAG1 in the presence or absence of NOTCH inhibitors, and multiplexed quantitative proteomics analysis of conditioned media identified proteins whose secretion responds to NOTCH signaling manipulation. This analysis identified 875 secreted factors, 129 of which showed significant expression changes after NOTCH manipulation; moreover, we validated the protein expression data through comparison with qRT-PCR and RNA profiling results from MEEC. NOTCH activation correlated directly with increased secretion of extracellular matrix (ECM) remodeling and structural proteins (TGFβ2 and collagens) and inversely with molecules involved in cellular migration/chemotaxis and protein-modifying enzymes. Specifically, DLL4-NOTCH signaling showed a major contribution to EMT, cytoskeleton signaling, and cell-cell/cell-matrix contacts, whereas JAG1-NOTCH signaling revealed a greater involvement in ECM deposition. Validation by *in situ* hybridization revealed specific valve endocardium and mesenchyme expression of selected candidate molecules in wild-type mouse embryos and their altered expression in NOTCH mutants. These findings coincide with the early role described for DLL4-NOTCH1 signaling in the promotion of EMT and cell migration and with a later role for JAG1-NOTCH1 in the regulation of valve mesenchyme proliferation and remodeling (13). These results affirm the value of MEEC as a powerful *in vitro* model for studying the endocardial secretome and identify novel factors potentially involved in heart valve development and disease.

EXPERIMENTAL PROCEDURES

Isolation and Immortalization of MEEC—MEEC were obtained and immortalized as described in (10).

Cell Culture—MEEC were cultured on 0.1% gelatin-coated 10-cm dishes and maintained in Dulbecco's modified Eagle's medium (DMEM) (Gibco) supplemented with 10% fetal bovine serum (FBS)

and 1% penicillin/streptomycin. Human umbilical vein endothelial cells were purchased from Lonza, and cultured on 0.1% gelatin-coated 10-cm dishes in Endothelial Cell Growth Medium-2 (EGM-2) with supplements (Lonza) and 1% penicillin/streptomycin. Mouse embryonic fibroblasts were obtained from E9.5 embryos disaggregated with a 1-ml syringe plunger and were plated in DMEM with high glucose and L-glutamine (Gibco), 15% FBS, 1 mM sodium pyruvate (Sigma-Aldrich), 0.1 mM β-mercaptoethanol (Sigma-Aldrich), and 1% penicillin/ampicillin. All cell lines were incubated at 37 °C in a humidified atmosphere containing 5% CO_2.

Calcium Ionophore Treatment—MEEC cultured on 0.1% gelatin-coated glass coverslips were exposed to 1 μM A23187 calcium ionophore (#C5149 Sigma-Aldrich) or DMSO (vehicle) (Sigma-Aldrich) for 6 h at 37 °C prior to fixation.

Immunocytochemistry—Confluent cells cultured on 0.1% gelatin-coated glass coverslips were fixed in 4% paraformaldehyde for 10 min at room temperature. MEEC were incubated with primary antibodies for 1 h at room temperature, followed by incubation for 1 h with a fluorescent-dye-conjugated secondary antibody. Antibodies used in this study were as follows: anti-ERG (Abcam EPR3863, 1:100); Alexa Fluor-488 conjugated goat anti-rabbit IgG (H+L) (Thermo-Fisher A-11034, 1:200); anti-NFATc1 (7A6; Enzo ALX-804-022-R100, 1:100); and goat anti-Mouse IgG (H+L) Alexa Fluor-488 conjugate (ThermoFisher A-11029, 1:100). Alexa Fluor-488-conjugated Isolectin GS-IB4 from *Griffonia simplicifolia* (ThermoFisher I32450, 1:200) was incubated for 4 min at room temperature prior to fixation. Fluorescein isothiocyanate-labeled phalloidin (Sigma-Aldrich P5282 1:200) was used to label actin filaments. Images were obtained with a NIKON A1R confocal fluorescence microscope and an Olympus BX51 fluorescence microscope.

Matrigel-based Tube Formation Assay—Each well of a 24-well plate was coated with 300 μl Growth Factor Reduced Matrigel (BD Biosciences 354230) at 4 °C, and the Matrigel was allowed to polymerize at 37 °C for 30 min. MEEC were treated with VEGF (R&D Systems 293-VE, 20 ng/ml) for 1 week, and 5×10^4 or 7.5×10^4 cells per well were added in DMEM and incubated for 6 h at 37 °C. Tube-like structures were observed with the Nikon Eclipse TS100 Inverted Microscope and photographed using the Nikon Digital Sight DS-2MBWc camera. Each condition was tested in duplicate.

NOTCH Stimulation with Recombinant Ligands—Recombinant NOTCH ligands DLL4-His (R&D Systems 1389-D4-050) and JAG1-Fc (R&D Systems 599-JG-100) were attached to 10-cm dishes as described in (14). MEEC (2.9×10^6 cells/plate) were seeded in DMEM supplemented with 10% FBS and treated with 20 μM of the γ-secretase inhibitor RO4929097 (Selleck Chemicals S1575): to inhibit NOTCH signaling, or DMSO (vehicle) for 24 h at 37 °C. The cells were washed twice with PBS and incubated for an additional 14 h in serum-free DMEM together with RO4929097 or DMSO as appropriate. Each condition was performed in triplicate.

Quantitative RT-PCR—RNA from MEEC stimulated with NOTCH recombinant ligands was extracted using the Direct-zol RNA Miniprep Kit (Zymo Research). cDNA was synthesized using the High Capacity Reverse Transcription Kit (Applied Biosystems), with 1 μg total RNA per reaction. Quantitative PCR was performed using Power SYBR™ Green Master Mix (Applied Biosystems 4367659) with the 7900HT Fast Real-Time PCR System (Applied Biosystems). Relative expression was determined using *Gapdh* or *β-Actin* as housekeeping genes. Mouse KiCqStart™ primer sequences (Sigma-Aldrich) used in this study are listed in Table S8. Three technical experiments were performed in each biological triplicate. Data are presented as mean ± s.d. Differences were considered statistically significant at $p < 0.05$ (two-tailed Student's *t* test).

Collection of Conditioned Media—Conditioned media from confluent serum-starved MEEC was collected by gentle aspiration and

---

[1] The abbreviations used are: AVC, atrio-ventricular canal; BMP2, bone morphogenetic protein 2; ECM, extracellular matrix; EMT, epithelial-mesenchymal transition; ERG, ets-related gene; FASP, filter aided sample preparation; HCD, higher-energy collisional dissociation; HUVEC, human umbilical vein endothelial cells; KEGG, kyoto encyclopedia of genes and genomes; LC-MS proteomics, Liquid Chromatography Mass Spectrometry proteomics; MECC, mouse embryonic endocardial cells; PCA, principal component analysis; TGFβ2, transforming growth factor beta 2; WSPP, weighted spectrum, peptide and protein.

centrifuged at 1200 rpm for 5 min to remove cell debris. The clear supernatant was immediately frozen in liquid nitrogen and then stored at -80 °C until proteomic analysis.

Experimental Design and Statistical Rationale—MEEC were stimulated with DLL4 or JAG1 in the presence of DMSO (vehicle) or RO4929097, and only DMSO represented the control condition (Fig. 1A). Conditioned media from these five experimental conditions were analyzed in biological triplicates in two independent tandem mass tag (TMT) 10-plex experiments (Fig. S2A). One TMT was used to study stimulation by DLL4 and the other to study stimulation by JAG1. Each TMT contained 3 controls (in DMSO, which were the same in both TMT experiments); 3 samples with the corresponding NOTCH ligand; 3 samples with the corresponding NOTCH ligand and RO4929097; and a common pool of all 15 samples was used as an internal control (Fig. S2A). The three biological replicates of each condition showed reproducible changes and clustered together into the same groups (see, for instance, Fig. 2A). Quantitative information from TMT reporter intensities was integrated from the spectrum level (Table S1), to the peptide level, and then to the protein level based on the weighted spectrum, peptide and protein (WSPP) statistical model (15, 16) using the generic integration algorithm (17). Briefly, for each sample r, the values $x_{qps} = \log_2 A_i/C$ were calculated, where A_i is the intensity of the TMT reporter of the corresponding sample i in the MS/MS spectrum s coming from peptide p and protein q, and C is the intensity of the TMT reporter from the internal control. The log2-ratio of each peptide (x_{qp}) was calculated as the weighted mean of its spectra, the protein values (x_q) were the weighted mean of its peptides, and the grand mean ($\bar{x}$) was calculated as the weighted mean of all the protein values (15). The statistical weights of spectra, peptides, and proteins (w_{qps}, w_{qp}, and w_q, respectively) and the variances at each one of the three levels (σ_S^2, σ_P^2, and σ_Q^2, respectively), were calculated as described (15). Protein abundance changes are expressed in standardized units (z_q). Built-in routines from the SanXoT package (18) were used to confirm that the z_q variables from each one of the samples followed strict normal N (0, 1) distributions, as expected from the WSPP model (17). Significant protein abundance changes across the different samples were detected by applying Student's t test to z_q data, and differences were considered statistically significant at $p < 0.05$.

LC-MS Proteomics—Proteins from the conditioned media were digested overnight at 37 °C in filter aided sample preparation filters with trypsin (Promega, Madison, WI, USA) at a 40:1 protein:trypsin (w/w) ratio in 50 mM ammonium bicarbonate, pH 8.8. The resulting peptides were desalted with C18 Oasis cartridges (Waters Corporation, Milford, MA, USA), using 50% acetonitrile (v/v) in 0.1% trifluoroacetic acid (v/v) as eluent, and vacuum-dried. The peptides were TMT labeled following manufacturer's instructions. Labeled peptides from each TMT experiment were pooled, separated into six fractions by mixed-cation exchange chromatography (Oasis HLB-MCX columns), desalted, and analyzed using a Proxeon Easy nano-flow HPLC system (Thermo Fisher Scientific, Bremen, Germany) coupled via a nanoelectrospray ion source (Thermo Fisher Scientific) to an Orbitrap Fusion mass spectrometer (Thermo Fisher Scientific). C18-based reverse-phase separation was used with a 2-cm trap column and a 50-cm analytical column (EASY column, Thermo Fisher Scientific) in a continuous acetonitrile gradient consisting of 0–30% A for 180 min, 50–90% B for 3 min (A = 0.1% formic acid; B = 90% acetonitrile, 0.1% formic acid) at a flow rate of 200 nl/min. Mass spectra were acquired in a data-dependent manner, with an automatic switch between MS and MS/MS using a top 15 method. MS spectra in the Orbitrap analyzer were in a mass range of 400–1500 *m/z* and 120,000 resolution. Higher-energy collisional dissociation fragmentation was performed at 35 eV of normalized collision energy and MS/MS spectra were analyzed at 30,000 resolution in the Orbitrap.

All searches were performed with Proteome Discoverer (version 1.4, Thermo Fisher Scientific) using SEQUEST (Thermo Fisher Scientific) against an Uniprot database containing all sequences from mouse (December 2015; 16,747 entries) and supplemented with 116 sequences from the cRAP database, containing the most common laboratory protein contaminants (Global Proteome Machine). For database searching, parameters were selected as follows: trypsin digestion with two maximum missed cleavage sites, precursor mass tolerance of 2 Da, fragment mass tolerance of 30 ppm. Methionine oxidation ($+15.994915$) was set as a variable modification. Lysine and peptide N-terminal modification of $+229.162932$ Da, as well as cysteine carbamidomethylation of $+57.021464$ Da, were set as fixed modifications. The same MS/MS spectra collections were also searched against inverted databases constructed from the same target databases. Peptide identification from MS/MS data was performed using the probability ratio method (19). False discovery rates of peptide identifications were calculated using the refined method (20, 21) a 1% false discovery rate was used as the peptide identification criterion. Each peptide was assigned only to the best protein proposed by the Proteome Discoverer algorithm. The whole set of identified peptides and proteins is shown in Table S1.

Bioinformatic Filtering of Secretory Proteins—The computational prediction of protein secretion was done as in (22) and is shown in Fig. 1D and Table S2. Briefly, from all the identified proteins at false discovery rate <1%, a list of potentially secreted proteins that met at least one of the following three criteria was constructed: (1) proteins annotated as extracellular by the DAVID v.6.7 website for Gene Ontology (GO) localization; (2) from the list of proteins not fulfilling the criteria in (1), proteins containing more than two transmembrane helices predicted by the TMHMM v.2.0 server (23), and a signal peptide according to the SignalP v.4.1 server. Those were termed as potentially secreted via the classical pathway; (3) proteins not fulfilling the criteria in (2) that had a SecretomeP v.2.0 score >0.5. Proteins in category (2) were classified as potentially secreted via the classical pathway; proteins in category (3) were classified as potentially secreted by a nonclassical pathway (24). To prevent overlap among secretion criteria, proteins were listed only under one category.

Data Representation—Principal component analysis was performed using ClustVis (https://biit.cs.ut.ee/clustvis/) (25) on the 690 secreted proteins common to the DLL4- and JAG1-specific datasets. Heatmaps were generated in ClustVis. Volcano plots were represented using a python custom script with the Matplotlib library, and protein names were added manually.

GO and KEGG Pathway Enrichment Analysis—GO and Kyoto encyclopedia of genes and genomes (KEGG) Pathway enrichment analyses of differentially secreted proteins were performed in GO-Elite (www.genmapp.org/go_elite/; 1.2.5, EnsMart77Plus database version) (26) with a permuted p value cutoff $p < 0.05$. We used the set of 690 proteins identified in both mixes as background, except for the network analysis, where we used the NOTCH-dependent endocardial secretome (129 differentially secreted proteins). Bar charts representing the z-score values of the terms in each category (biological process, cellular component, molecular function, and KEGG pathways) were generated with GraphPad Prism 7.

Network Analysis of Proteomic Data—The 129 differentially secreted proteins showing differential regulation after global NOTCH pathway activation/inhibition, served as input node data for the STRING 11.0 database (http://string-db.org/) (27). To obtain more stringent interactions, the *Textmining* option in STRING was excluded, and the minimum required interaction score considered was 0.7 (high confidence). Resulting networks were then replotted using Cytoscape 3.7.1 (www.cytoscape.org/) (28), by applying the Prefuse

Force Directed Layout setting for the global analysis. The significance of the predicted network was assayed using as background the set of 690 proteins identified in both mixes.

Tissue Processing and In Situ Hybridization (ISH)—Embryos were fixed in 4% paraformaldehyde at 4 °C overnight. Embryos older than E10.5 were paraffin embedded following standard protocols. ISH and whole-mount *ISH* were performed as described (29, 30). Details of probes will be provided on request.

Mouse Strains and Genotyping—Animal studies were approved by the CNIC Animal Experimentation Ethics Committee and by the Community of Madrid (Ref. PROEX 118/15). All animal procedures conformed to EU Directive 2010/63EU and Recommendation 2007/526/EC regarding the protection of animals used for experimental and other scientific purposes, enforced in Spanish law under Real Decreto 1201/2005. Mouse strains used in this study were *Tie2-Cre* (31), *Nkx2.5-Cre* (32), *Dll4flox* (33), and *Jag1flox* (34). Details of genotyping have been published for *Dll4flox;Tie2-Cre* (10), *and Jag1flox;Nkx2.5-Cre* (13).

RESULTS

MEEC Show Features of Embryonic Endocardium—To investigate the NOTCH-dependent endocardial secretome, we used a previously generated MEEC line (10). Morphological examination revealed a cobblestone-like morphology resembling that of human umbilical vein endothelial cells, contrasting the elongated shape of mouse embryonic fibroblasts (Fig. S1A). MEEC showed positive staining with the endothelial surface marker isolectin B4 (35) (Fig. S1B) and for immunodetected ERG in the nucleus (36) (Fig. S1C). The endocardial marker NFATc1 was diffusely expressed in the cytoplasm (Fig. S1D) and translocated to the nucleus after the addition of a Ca^{2+} ionophore (37) (Fig. S1E). We tested the angiogenic behavior of VEGF pretreated MEEC in an endothelial tube formation assay on reduced growth factor Matrigel (38). In response to angiogenic stimulation for 6 h, MEEC aligned and formed capillary-like structures within the Matrigel, and the tube network was more extensive after a higher initial seeding density (Figs. S1F and S1G). These results indicate that MEEC retain properties of embryonic endocardial cells and are thus an appropriate *in vitro* system in which to manipulate endocardial NOTCH signaling.

Analysis of the NOTCH-dependent Endocardial Secretome—To achieve ligand-specific NOTCH signaling activation or inhibition, we stimulated MEEC with immobilized recombinant DLL4 or JAG1 ligands (14) in the presence of DMSO (vehicle) or the γ-secretase inhibitor RO4929097 (RO) (Fig. 1A). This allowed us to compare the ligand-specific NOTCH-dependent secretome in activating and inhibitory conditions. NOTCH activation and abrogation were confirmed by qRT-PCR of the NOTCH target genes *Hey1*, *Hey2*, *HeyL*, and *Nrarp* (39–41) (Figs. 1B and 1C).

Serum-free conditioned media from each experimental condition was analyzed by protein digestion followed by multiplexed isobaric labeling and analysis by LC-MS/MS (Fig. S2A, see "Experimental Procedures"), resulting in the identification of peptides from nonredundant proteins across all experimental conditions (Fig. 1D and Table S1). Based on

features that are shared among secreted proteins, they were filtered by stringent computational analysis to select those likely to be exported by live cells as soluble proteins. A final list of 875 candidate defined the endocardial secretome (Fig. 1D and Table S2). Principal component analysis of the secretome response revealed a treatment-based separation into three clusters: ligand-driven NOTCH activation, NOTCH inhibition, and nonstimulation (control) (Fig. S2B). Treatment triplicates showed an overall superposition, and the only three outliers were included in the following statistical analysis.

Altogether, we achieved a meaningful stimulation and inhibition of NOTCH signaling in MEEC, allowing selection of potentially secreted proteins representing the NOTCH-dependent endocardial secretome.

NOTCH Signaling Regulates Growth Factors and Extracellular-Matrix Component Secretion—To study the overall effect of NOTCH activation in the endocardial secretome composition, we focused on the 690 secreted proteins (78.6% of the total) identified after both JAG1- and DLL4-stimulation (Fig. S2C and Table S3A). Within this group, we selected only secreted proteins showing significant changes ($p < 0.05$) after global NOTCH activation or inhibition (Table S3B). To this end, we compared NOTCH activation (DLL4- and JAG1-DMSO combined) *versus* NOTCH inhibition (DLL4- and JAG1-RO combined), and NOTCH activation *versus* control (DMSO) and NOTCH inhibition combined (Figs. S3A and S3B). Proteins showing differential secretion in at least one comparison were selected ($n = 129$). Hierarchical clustering of these common proteins by secretion pattern yielded four major groups (Fig. 2A), corresponding to proteins hyposecreted or hypersecreted after NOTCH inhibition (clusters 1 and 4; Fig. 2A) and to proteins hyposecreted or hypersecreted after NOTCH activation (clusters 2 and 3; Fig. 2A).

To better understand the functions of these NOTCH-responsive proteins, we conducted GO enrichment analysis of the two major secretome profiles, based on hypersecretion (clusters 1 and 3; Fig. 2A) and hyposecretion (clusters 2 and 4; Fig. 2A) during NOTCH activation. The analysis showed that the first group (59 proteins) had significant overrepresentation of ECM-remodeling and collagen-related terms, in which several components of the ECM (TGFβ2, CTGF, FBLN2, FN1, and a variety of collagens) and remodeling enzymes (lysyl-oxidase -LOX- and metalloproteinase inhibitors -TIMP1 and TIMP3–) were included (Fig. 2B and Table S5A). In contrast, the second group (70 proteins) showed enrichment in semaphorin signaling and protein modification terms, including ubiquitin-conjugating enzymes (NEDD4, UBE2K, and UBE2V1), aminopeptidases (NPEPPS, PEPD, XPNPEP1), and metalloproteinases (ADAM10, ADAMTS5, AEBP1) (Fig. 2C and Table S5A). Similar results were obtained with KEGG pathway analysis, further supporting the notion that NOTCH stimulation promotes the secretion of paracrine signals involved in "ECM-receptor interaction," "focal adhesion," "pathways in cancer," and "TGFβ signaling," which are
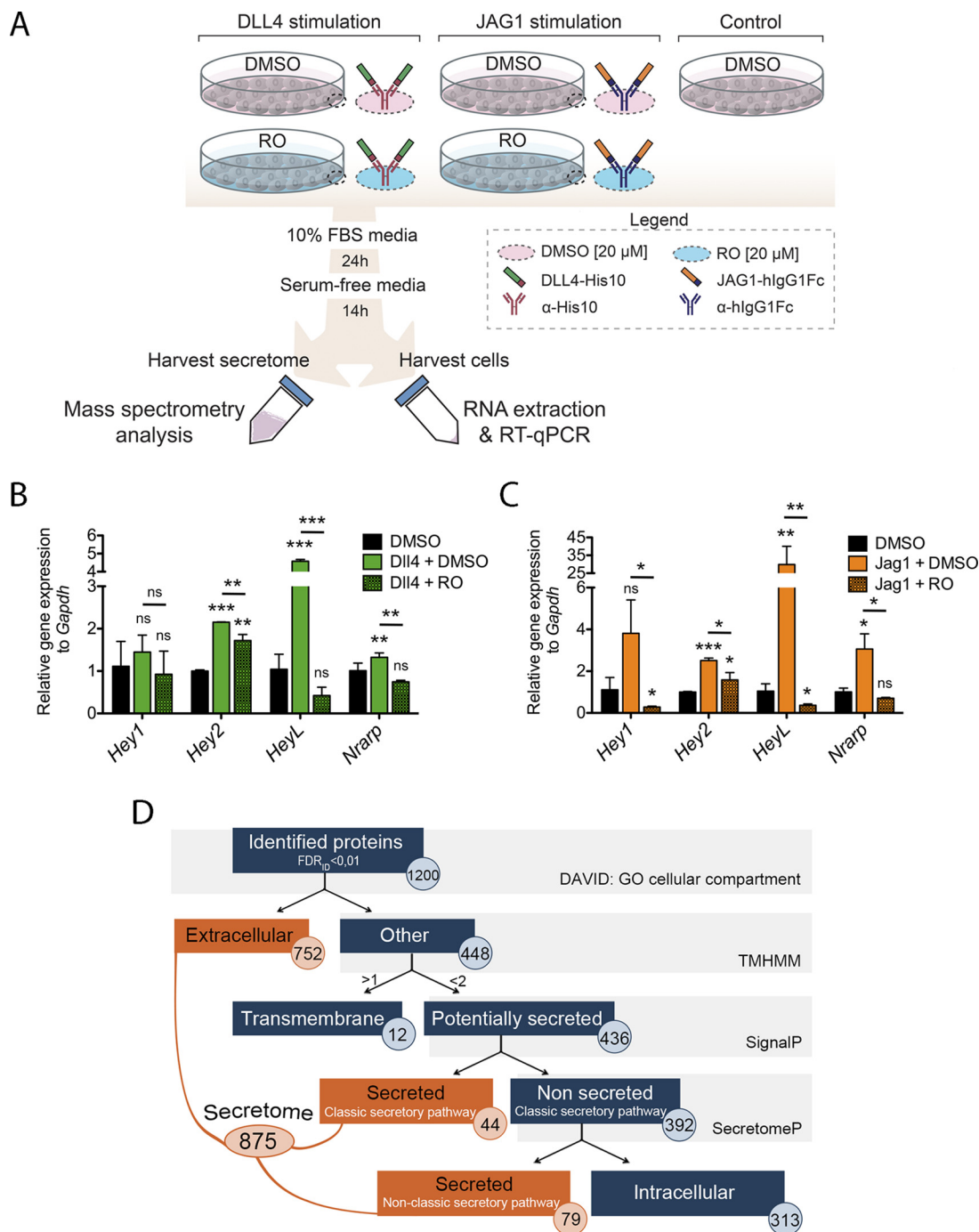
FIG. 1. **Profiling the endocardial-derived secretome through *in vitro* modulation of the NOTCH pathway in MEEC.** (*A*) Experimental design of MEEC proteome analysis. MEEC were stimulated with the recombinant NOTCH ligands DLL4-His10 (green) or JAG1-hIgG1Fc, in combination with vehicle (DMSO) or the γ-secretase inhibitor RO4929097 (RO). At the end of the treatment period, cells were collected for qRT-PCR analysis and protein content in conditioned media was analyzed by LC-MS/MS. (*B*, *C*) qRT-PCR analysis of canonical Notch target genes *Hey1*, *Hey2*, *HeyL*, and *Nrarp* in DLL4-stimulated MEEC (*B*) and JAG1-stimulated MEEC (*C*). Data are means of triplicate measures of each sample and are presented as mean ± s.d. (Student's *t* test; *$p < 0.05$; **$p < 0.01$, ***$p < 0.005$). (*D*) Workflow of sequential bioinformatics analysis with the DAVID, TMHMM, SignalP, and SecretomeP servers to identify secreted proteins. Circles show the number of proteins in each group; orange indicates secreted proteins.

closely associated with cellular migration and invasiveness and with diminished secretion of guidance/chemotaxis signals, like semaphorins (Figs. 2*B* and 2*C*).

To identify the protein-protein interactions underlying the functions described above, we constructed the interactome of the NOTCH-dependent endocardial secretome by integrat-
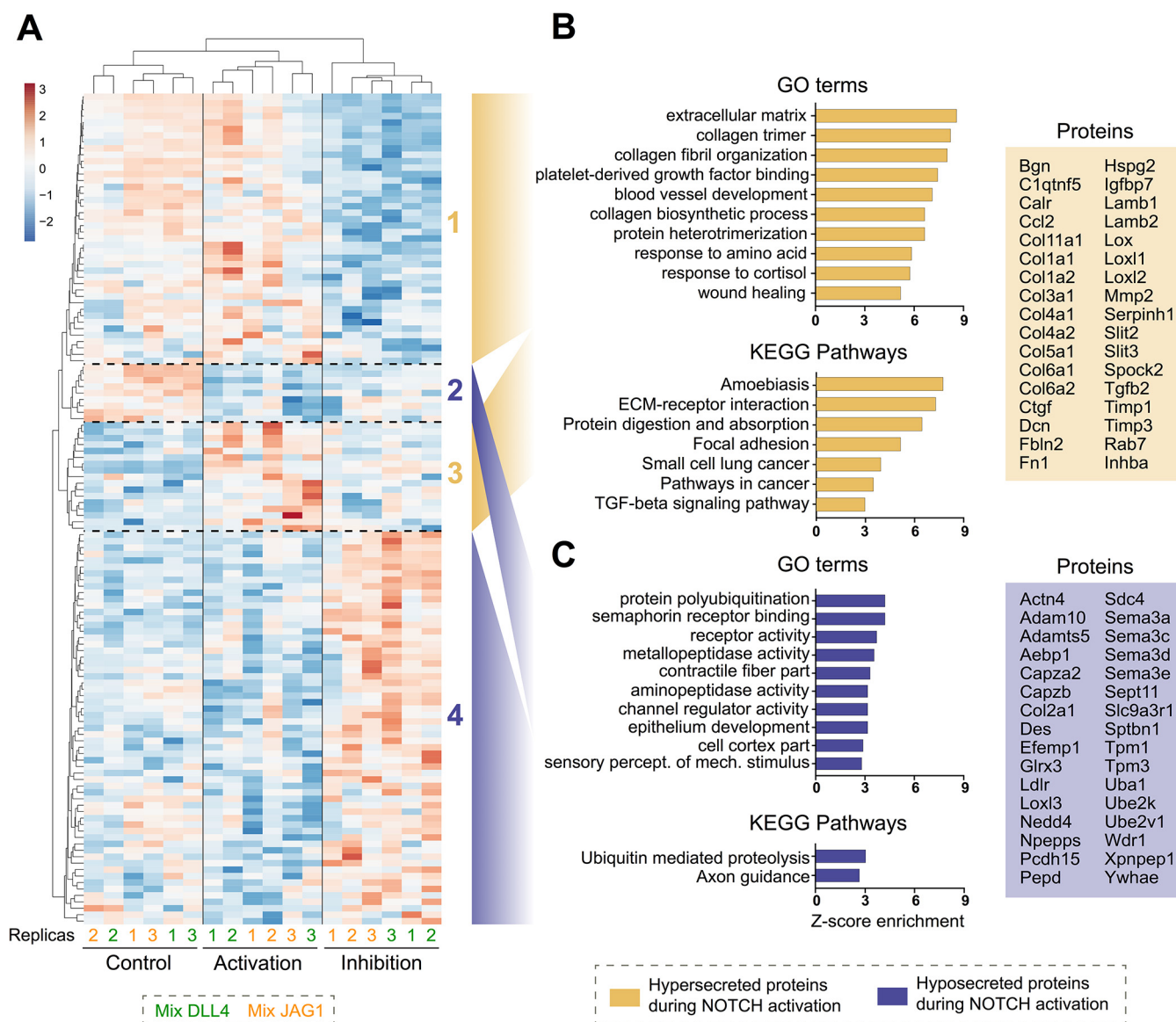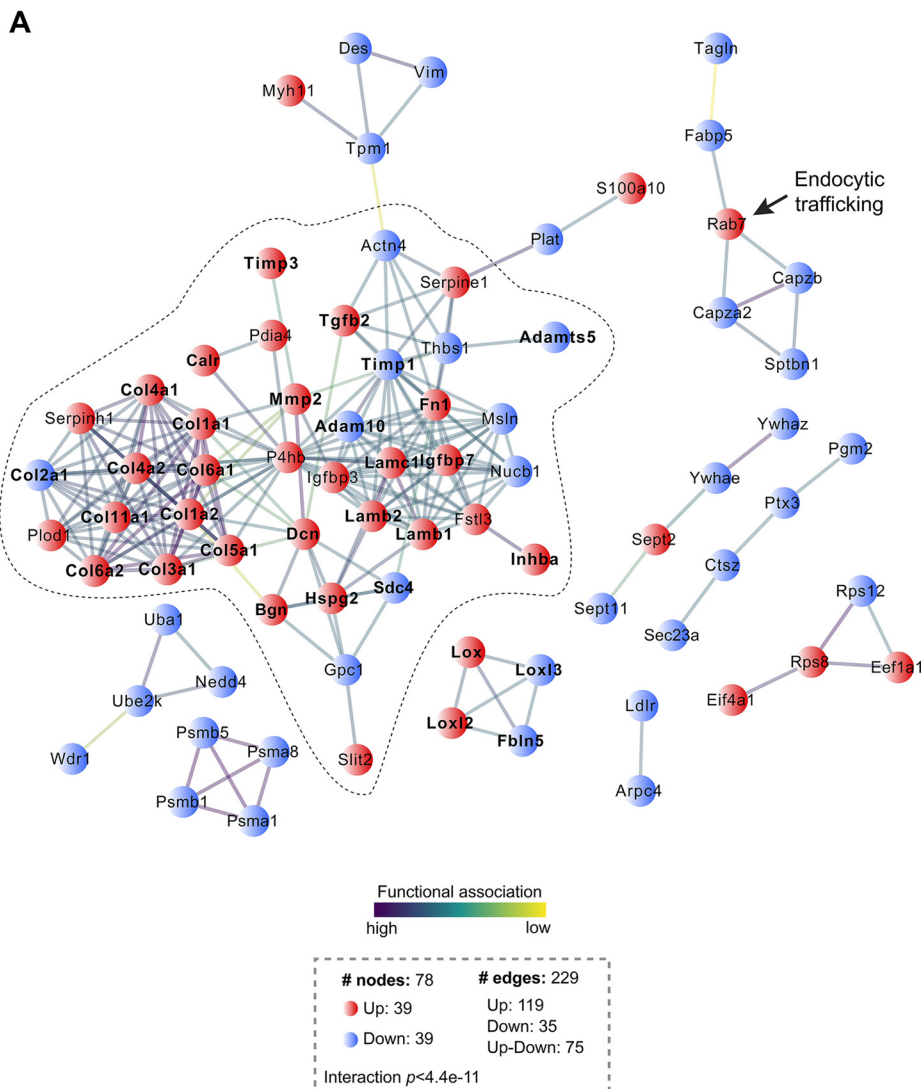
FIG. 2. **Global NOTCH-associated secretory profile.** (A) Hierarchical clustering of the 129 secreted factors displaying significant abundance changes (t test, p < 0.05) in comparisons of NOTCH activation *versus* inhibition or of NOTCH activation *versus* the combination of control plus inhibition. Dashed lines mark the delineation of four clusters; yellow clusters (1, 3) show increased abundance upon NOTCH activation; purple clusters (2, 4) show decreased abundance upon NOTCH activation. (B, C) Charts showing enrichment analysis for GO terms and KEGG pathways for proteins hypersecreted (B) or hyposecreted (C) in response to NOTCH activation. Colored boxes show names of secreted factors in each cluster pair.

ing the 129 differentially expressed proteins with the STRING v11 database (26) (Table S6A). We predicted a statistically significant network containing 78 nodes (39 hypersecreted and 39 hyposecreted) connected by 229 edges representing physical or functional interactions (Fig. 3A and Table S6B). We identified two major clusters containing the most densely connected nodes (enclosed by a dotted line in Fig. 3A) in which 29 out of 39 nodes corresponded to hypersecreted proteins. Among them, the most interconnected proteins were structural proteins (collagens) and ECM-remodeling factors (bold names in Fig. 3A). These proteins appeared in the most

represented GO terms and KEGG pathways, which corresponded with extracellular matrix, collagen organization, response to stimulus, ECM-receptor interactions, and focal adhesion. The other nodes were mostly hyposecreted proteins forming poorly interconnected networks. Interestingly, we found an increase in RAB7 levels, a key regulator in the endo-lysosomal trafficking, suggesting that NOTCH might also mediate a cross-talk to the neighboring cells through the release of signals that are packaged into vesicles (42).

Overall, our analysis indicated that NOTCH-mediated paracrine signaling in the endocardial secretome modulated TGFβ

FIG. 3. **Interactome of NOTCH-associated secretory profile.** (A) NOTCH-dependent interactome, showing 78 nodes (differentially secreted proteins in at least one comparison: NOTCH activation *versus* inhibition, or NOTCH activation *versus* the combination of control plus inhibition. The nodes are connected by 229 edges (physical or functional interactions). The purple-yellow gradient of the edges reflects their degree of interaction (from high to low). Dashed lines delineate those nodes forming the most densely connected clusters. Red and blue indicate higher and lower secretion upon NOTCH activation, respectively. Bold names represent ECM-remodeling proteins.

signaling, focal adhesion, and ECM formation to regulate cellular movements during cardiac development.

DLL4 and JAG1 Ligands Determine a Distinct Secretome Composition—During heart valve development, DLL4 and JAG1 act sequentially to activate NOTCH signaling. Early endocardial DLL4-NOTCH activity drives the EMT that will lead to the formation of the valve primordium. Later on, JAG1-NOTCH signaling is crucial for the regulation of valve mesenchyme cell proliferation (13). To determine whether DLL4 and JAG1 elicit different protein secretion responses in MEEC, we compared the secretomes obtained after stimulation with JAG1 and DLL4, using the same statistical analysis as in the previous section. JAG1-mediated stimulation altered the secretion of 82 proteins, whereas DLL4 altered the secretion of 113 proteins (Fig. 4*A* and Tables S4*A* and S4*B*). Only 24 proteins were altered in both JAG1- and DLL4-stimulated MEEC. Thus, 70–80% of the differentially secreted proteins were ligand specific. To visualize the changes in protein abundance, we performed a hierarchical clustering of the JAG1-

and the DLL4-dependent secretome (Figs. 4*B*–4*D*). Hypersecretion (compared with the control and RO situations) was the main effect in the JAG1-dependent secretome; in contrast, with DLL4 stimulation, the main effect was hyposecretion. Interestingly, most of the 24 secreted proteins altered in both JAG1- and DLL4-stimulated MEEC responded similarly to both ligands (clusters 1 and 3 in Fig. 4*D* and Table S4*C*).

To associate specific functions to each ligand, we focused on those clusters showing major protein-level alterations after ligand activation (dashed boxes in Figs. 4*B* and 4*C*). We distinguished between proteins identified as hypersecreted (yellow dashed box in Figs. 4*B* and 4*C*) and hyposecreted (purple dashed box) in the JAG1- or the DLL4-specific secretome. GO and KEGG pathway analysis of these clusters revealed distinct biological functions associated with each ligand (Fig. 4*E* and Table S5*B*). Proteins whose secretion was reduced after DLL4 activation (Fig. 4*C*) belonged to the GO terms "glucose metabolic processes," "cellular component disassembly," and "regulation of blood circulation," whereas

hypersecreted proteins were related to "cell-cell junction organization" (DSP, JUP), "organelle organization," or "cell development" (TGFβ2). In contrast, the most enriched terms among the JAG1-specific hypersecreted proteins (Fig. 4B) were "platelet-derived growth factor binding," "regulation of cartilage and blood vessel development," and "collagen fibril organization" (collagens), whereas hyposecreted proteins were involved in "semaphorin receptor binding" (semaphorins) (Fig. 4E and Table S5B). Thus, DLL4 seems to affect the secretion of proteins playing a role in cellular metabolism, cell adhesion, and cytoskeletal dynamics, whereas JAG1 leads to changes in ECM structure and semaphorins. These results showed that stimulation with DLL4 and JAG1 triggered different secretome responses in MEEC, likely reflecting the different roles played by these ligands during heart valve development.
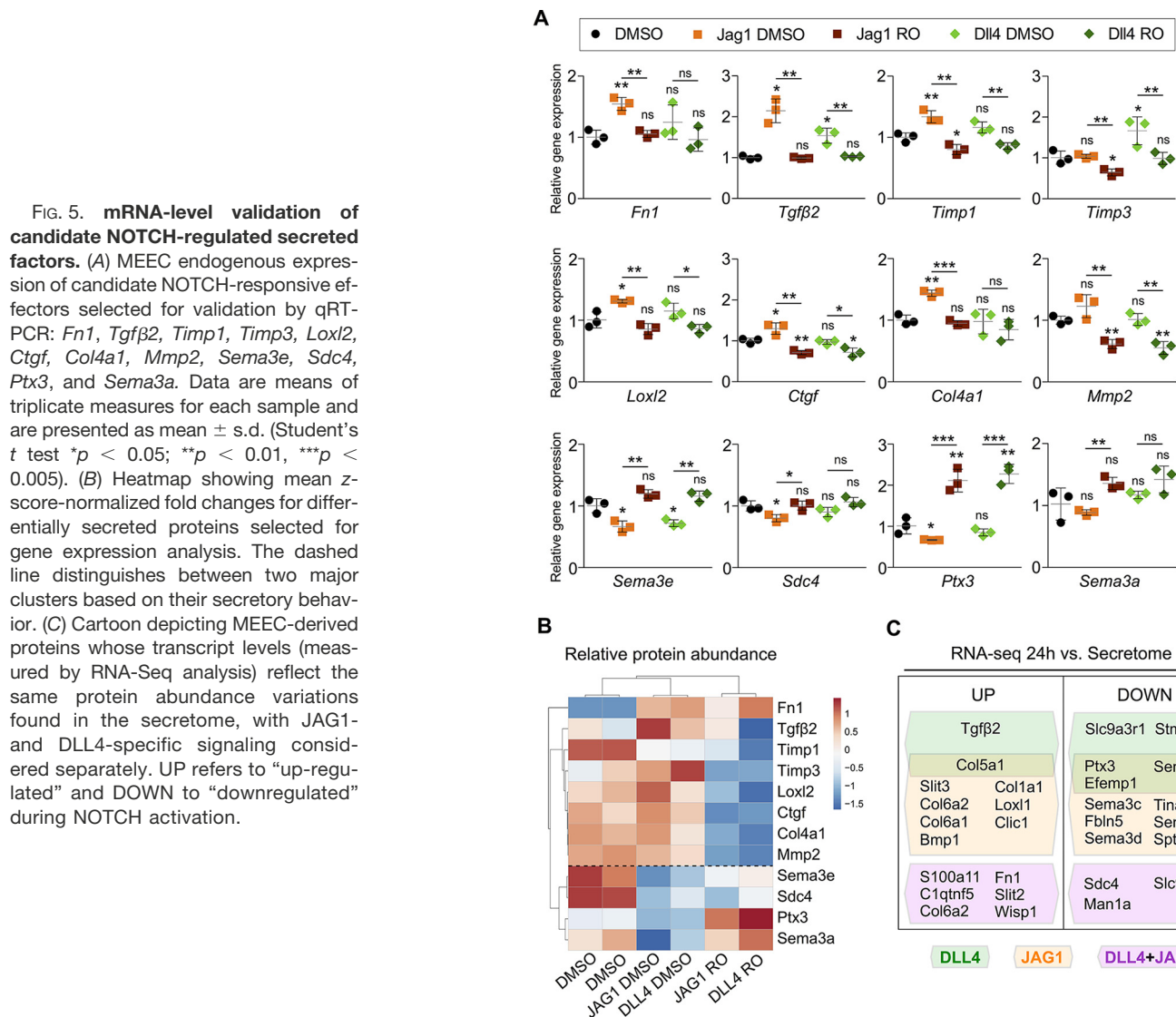
NOTCH-driven Gene Expression Correlates with Protein Secretion—To validate the secretome data, we examined whether the protein secretion changes after NOTCH stimulation or inhibition in MEEC were accompanied by similar changes in mRNA expression. Thus, we analyzed the expression of NOTCH-responsive proteins representing the most enriched GO categories by qRT-PCR (Fig. 5A). In the case of genes encoding proteins hypersecreted when comparing NOTCH activation *versus* NOTCH inhibition, we found that JAG1 enhanced the transcription of *Fn1*, *Tgfβ2*, *Col4a1*, and *Ctgf*, molecules related to ECM remodeling and EMT, as well as the ECM-remodeling enzymes *Timp1*, *Timp3*, *Mmp2*, and *Loxl2*, whereas DLL4 stimulation up-regulated *Tgfβ2* and *Timp3* (Fig. 5A). In agreement with the secretome data (Fig. 5B), all these genes were downregulated in the presence of RO (Fig. 5A). Opposite results were obtained for *Sdc4*, *Ptx3*, *Sema3a*, and *Sema3e*, which were strongly up-regulated upon NOTCH abrogation (Fig. 5A). Further, we compared the secretome data with available transcriptomic data from MEEC co-cultured for 24 h with DLL4- or JAG1-expressing OP9 cells (Luna-Zurita, MS in preparation). The comparison distinguished between secreted proteins with significant differences at the transcript or protein level, at the protein level or at both (Figs. S4A and S4B and Table S7A). Despite the relatively poor correlation between secretion and expression when comparing those significantly changed at least at one level ($r = 0.2953$ for JAG1 and $r = 0.1749$ for DLL4), we found a positive correlation when we focused on those proteins differentially secreted and expressed after NOTCH pathway activation ($r = 0.6965$ for JAG1 and $r = 0.6685$ for DLL4; Figs.

S4A and S4B and Table S7A). Some of the most functionally relevant proteins identified in our secretome data were among the proteins whose abundance changes were reflected at the transcript level (Tables S7B and S7C). This was the case for the hypersecreted/up-regulated factors TGFβ2, FN1, COL1A1, COL5A1, COL6A1, and COL6A2 and for the hyposecreted/downregulated factors SEMA3A, SEMA3C, SEMA3D, SEMA3E, SDC4, and PTX3 (Fig. 5C and Table S7D). These results showed a positive correlation between NOTCH-dependent protein secretion and mRNA expression levels and strongly suggest that NOTCH signaling alters protein secretion through transcriptional regulation.

In Vivo Validation of NOTCH-dependent Endocardial Secretome Candidates—During cardiac valve development, NOTCH drives the EMT that gives rise to the valves primordia (43) and later regulates mesenchyme proliferation and differentiation to generate the adult valves (13, 44, 45). Both of these processes require exquisite regulation of ECM production and maturation.

Given the prominent contribution of ECM-related proteins to the MEEC NOTCH-dependent secretome (Fig. 2B; Table S5), we examined developing mouse valves for the transcript expression of selected ECM-related molecules. Based on the transcriptomic and proteomic responses to NOTCH activation (Figs. 5A and 5B), we selected *Tgfβ2*, *Loxl2*, *Ptx3*, *Timp3*, *Fbln2*, and *Dcn* for the *in vivo* validation. TGFβ2 is a member of the TGFβ family that promotes endocardial cushion formation by EMT (46, 47). LOXL2 is an enzyme responsible for covalent crosslinking of ECM components (48). PTX3 is a cytokine involved in the conversion of mesenchyme cancer cells into epithelium (49). TIMP3 is the major inhibitor of matrix metalloproteinases (50). FBLN2 is a glycoprotein that plays a central role in matrix stabilization (51). Finally, DCN is a proteoglycan that interacts with collagens and free TGFβ to provide a structural scaffold in connective tissues (52). ISH revealed expression of these genes, with the exception of *Dcn* (data not shown), in the outflow tract (OFT) and atrioventricular canal (AVC) regions of the E10.5 mouse heart (Fig. S5A). Consistent with a previous report (47), *Tgfβ2* was expressed in AVC and OFT endocardium and mesenchyme and in the myocardium (Fig. S5A). However, *Loxl2*, *Ptx3*, *Timp3*, and *Fbln2* were confined to the endocardium and cushion mesenchyme (Fig. S5A). At E15.5, the AVC endocardial cushions have given rise to the atrioventricular valves (mitral and tricuspid) and the OFT cushions to the semilunar valves (aortic and pulmonary). *Loxl2*, *Ptx3*, *Timp3*, *Fbln2*, and *Dcn* were ex-

FIG. 4. **DLL4 and JAG1 elicit distinct secretory profiles.** (*A*) Venn diagram showing overlap of differentially secreted proteins (*t* test, $p < 0.05$) in at least one comparative analysis (NOTCH activation *versus* inhibition or NOTCH activation *versus* the combination of control plus inhibition), with JAG1-specific and DLL4-specific signaling considered separately. (*B–D*) Heatmaps showing *z*-score-normalized fold changes for proteins differentially secreted exclusively in response to signaling by JAG1 (*B*), DLL4 (*C*), or by both ligands (*D*), in at least one comparison. In *D*, protein names are given alongside each row, and the dashed line distinguishes between three major clusters based on their secretory behavior. (*E*) Heatmap showing the GO-Elite server-generated list of enriched GO terms and KEGG pathways for hypersecreted (yellow dashed line in *B* and *C*) and hyposecreted proteins (purple dashed line) in response to stimulation with JAG1 (orange) and DLL4 (green) stimulation. Color scale represents *z*-enrichment scores. Colored boxes show names of secreted factors in each cluster.

FIG. 5. **mRNA-level validation of candidate NOTCH-regulated secreted factors.** (*A*) MEEC endogenous expression of candidate NOTCH-responsive effectors selected for validation by qRT-PCR: *Fn1*, *Tgfβ2*, *Timp1*, *Timp3*, *Loxl2*, *Ctgf*, *Col4a1*, *Mmp2*, *Sema3e*, *Sdc4*, *Ptx3*, and *Sema3a*. Data are means of triplicate measures for each sample and are presented as mean ± s.d. (Student's *t* test *$p < 0.05$; **$p < 0.01$; ***$p < 0.005$). (*B*) Heatmap showing mean *z*-score-normalized fold changes for differentially secreted proteins selected for gene expression analysis. The dashed line distinguishes between two major clusters based on their secretory behavior. (*C*) Cartoon depicting MEEC-derived proteins whose transcript levels (measured by RNA-Seq analysis) reflect the same protein abundance variations found in the secretome, with JAG1- and DLL4-specific signaling considered separately. UP refers to "up-regulated" and DOWN to "downregulated" during NOTCH activation.

pressed in the endocardium and mesenchyme of the atrioventricular valves and OFT valves (Fig. S5B). These results showed that the selected MEEC secretome genes are expressed in cardiac tissues undergoing developmental processes in which the ECM plays a crucial role, such as valve morphogenesis.

We next assessed whether NOTCH pathway inactivation *in vivo* triggered the same gene expression changes observed in MEEC. At E9.5, DLL4 is essential for EMT and endocardial cushion formation in the AVC (13). We conditionally inactivated *Dll4* in the developing endothelium and endocardium by crossing mice bearing a conditional *Dll4^{flox}* allele (33) with the driver line *Tie2-Cre* (31). Whole-mount ISH analysis of E9.5 *Dll4^{flox};Tie2-Cre* mutant hearts revealed a severely reduced expression of *Tgfβ2* in the AVC region (endocardium and myocardium) (Figs. 6A and 6B), of *Loxl2* in the AVC endocardium (Figs. 6C and 6D), and of *Fbln2* in the AVC endocardium and mesenchyme (Figs. 6E and 6F). In contrast, expression of

Ptx3, *Dcn*, and *Timp3* was unaffected (data not shown). These findings are consistent with reports indicating that *Tgfβ2* is a NOTCH target during early valve development (4) and identify *Fbln2* and *Loxl2* as potential novel EMT mediators downstream of NOTCH. JAG1 regulates mesenchyme proliferation and differentiation during valve morphogenesis (13). To ablate *Jag1* throughout the myocardium and endocardium and its mesenchymal derivatives, leading to valve dysmorphology (13), we bred *Jag1^{flox}* mice (34) with the cardiac-specific *Nkx2.5-Cre* driver line (32). ISH analysis revealed that increased valve cellularity of *Jag1^{flox};Nkx2.5-Cre* mutant embryos at E14.5 was accompanied by altered expression of *Loxl2* (Figs. 6G–6H''), *Fbln2* (Figs. 6I–6J''), and *Ptx3* (Figs. 6K–6L''). However, *Tgfβ2*, *Timp3*, and *Dcn* remained unchanged (data not shown). In agreement with the secretome data (Fig. 4D and Table S4C), *Loxl2* and *Fbln2* mRNA were reduced in *Jag1^{flox};Nkx2.5-Cre* mutant valves (Figs. 6G–6J''), whereas *Ptx3* was up-regulated (Figs. 6K–6L''). This finding is
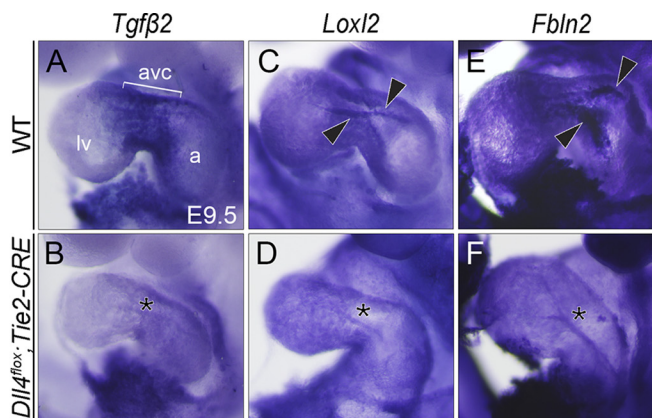
FIG. 6. *In vivo* validation of *Tgfβ2, Loxl2, Fbln2*, and *Ptx3* as NOTCH-target genes in NOTCH pathway mouse mutants. (*A–F*) Whole-mount ISH analysis in E9.5 WT and *Dll4*[flox]*;Tie2-Cre* embryos, showing a general view of the heart. *Tgfβ2* expression in AVC myocardium (*A*) is lost in mutants (*B*, asterisk). *Loxl2* expression in AVC endocardium (*C*, arrowheads) is decreased in mutants (*D*, asterisk). *Fbln2* expression in AVC endocardial and mesenchymal cells (*E*, arrowheads) is markedly downregulated in mutants (*F*, asterisk). (*G–L″*) ISH analysis in heart sections from E14.5 WT and *Jag1*[flox]*;Nkx2.5-Cre* embryos. Expression of *Loxl2* (*G–H″*) and *Fbln2* (*I–J″*) is lower in endocardial and mesenchymal cells of mutant atrioventricular valves, whereas *Ptx3* is up-regulated in mesenchymal cells (*K–L″*). Boxed areas are magnified in the panels on the right (′ tricuspid valve; ″ mitral valve). Scale bars: 100 μm. a (atria), avc (atrioventricular canal), ivs (interventricular septum), lv (left ventricle), mv (mitral valve), tv (tricuspid valve).
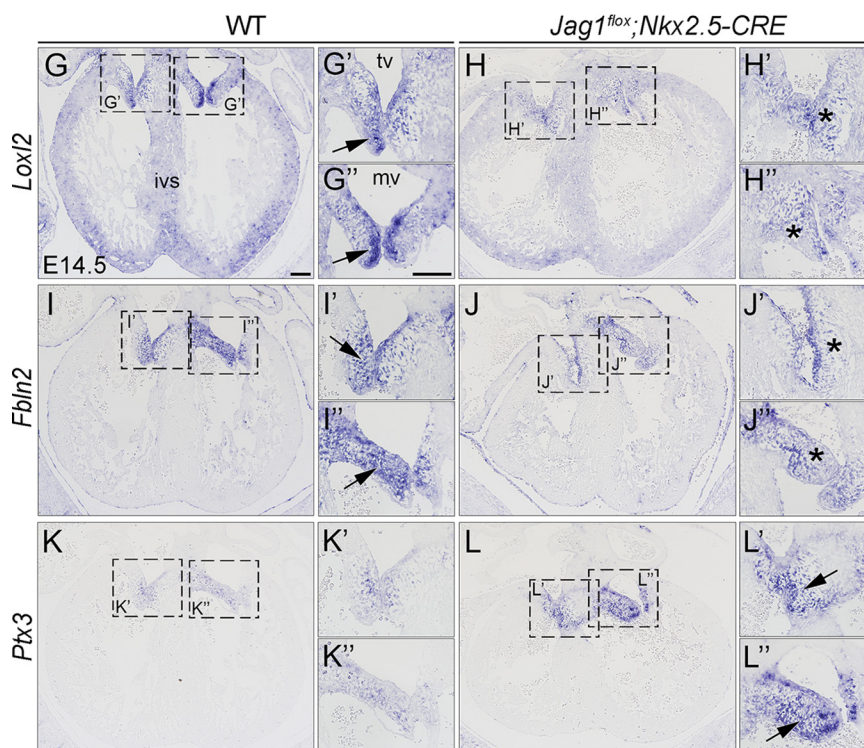
consistent with the secretome data (Table S4) and suggests a positive correlation between increased *Ptx3* transcription and the presence of excessive immature mesenchyme after JAG1-NOTCH signaling blockade (13). In summary, our results validate MEEC as a powerful *in vitro* model of endocardial cell signaling and support the potential of this *in vitro* system to identify molecules involved in valve morphogenesis.

DISCUSSION

We have generated an *in vitro* system to circumvent the severe limitation imposed on proteomic studies of early heart development by the tiny amounts of cardiac tissue available. Using MEEC, we have been able to identify for the first time the NOTCH-dependent embryonic endocardial secretome. MEEC have cellular and functional features of endothelium

(Isolectin B4 staining and ERG expression), showing a cobblestone appearance and an ability to form capillary-like structures in Matrigel. In addition, MEEC express a typical endocardial marker (NFATc1), demonstrating that they are a suitable *in vitro* experimental system in which to assay the effect of NOTCH-signaling manipulation on protein secretion, as well as for future investigation into endocardial cell biology.

We stimulated MEEC with the recombinant ligands DLL4 or JAG1, demonstrating NOTCH pathway activation and its inhibition in the presence of RO and examining target-gene expression by qRT-PCR in these settings. Quantitative proteomics analysis of conditioned media from the different experimental conditions identified proteins whose secretion responds to NOTCH manipulation. To analyze the proteome data, we combined advanced quantitative statistical models

(15, 17, 18) with various web-based interfaces, identifying 875 secreted factors, 129 of which underwent significant expression changes upon NOTCH manipulation. NOTCH activation correlated directly with an increased secretion of ECM remodeling and structural proteins (TGFβ2, collagens) and inversely with guidance signals (semaphorins) and protein-modifying enzymes. These results are consistent with the reported relationship in cardiovascular development between NOTCH, ECM dynamics, and semaphorins in cardiovascular development (53, 54) and indicate an additional level of regulation through protein secretion. The identified secretome profiles were ligand specific. DLL4-NOTCH signaling mostly stimulated the production of TGFβ2, intercellular junction proteins, and cytoskeletal proteins, suggesting an involvement in EMT, cell-cell/cell-matrix adhesion and cytoskeleton signaling. In contrast, JAG1-NOTCH signaling prompted higher levels of collagen-related proteins, indicating a major contribution to EMT and ECM deposition. These findings agree with the early role described for DLL4-NOTCH1 signaling in the promotion of EMT and cell migration *versus* the later role of JAG1-NOTCH1 in the regulation of valve mesenchyme proliferation and remodelling (13).

qRT-PCR validation of selected differentially secreted proteins identified in the MEEC secretome experiments revealed a marked correspondence between mRNA and protein secretion dynamics. This correlation between mRNA and protein secretion dynamics was confirmed by analysis of RNA-Seq data from DLL4- and JAG1-stimulated MEEC, strongly suggesting that protein delivery is influenced by a NOTCH-dependent transcriptional regulation. Participation of the NOTCH secretome in EMT and ECM dynamics was further validated by *in vivo* analysis of selected potential NOTCH-responsive genes (*Tgfβ2*, *Loxl2*, *Ptx3*, *Timp3*, *Fbln2,* and *Dcn*) expressed in the early (E10.5) and remodeling (E15.5) heart valve. Interestingly, *Tgfβ2* was previously described as a secreted NOTCH effector (4) mediating EMT initiation (55). The detection of this cytokine in the MEEC secretome thus not only highlights the sensitivity of our approach, but also indicates the appropriateness on the proteome dataset for exploring the EMT signaling cascade downstream of NOTCH. At early stages, *Loxl2*, *Ptx3*, *Timp3,* and *Fbln2* were restricted to endocardium and mesenchyme cells configuring the AVC cushions and the OFT, whereas *Tgfβ2* was also present in the myocardium of both territories, in agreement with previous publications (56). Later in development, *Dcn* and the remaining candidates were also expressed in the atrioventricular and semilunar valve leaflets. These results suggest that these factors contribute to valve development and may play distinct roles according to their differential spatio-temporal localization in the endocardium and mesenchyme. The relationship between NOTCH signaling and these paracrine factors was confirmed by analyzing their expression in *Dll4* and *Jag1* targeted mutants. *Tgfβ2*, *Loxl2*, and *Fbln2* transcripts were downregulated in E9.5 *Dll4^flox;Tie2-Cre* mutant hearts, in which EMT is impaired (13). A similar reduction in *Tgfβ2*

expression was previously reported in *RBPJκ* and *Notch1* mutants (43). These findings suggest that NOTCH1 activity may trigger the transcription and subsequent release of Loxl2 and Fbln2 signals from the endocardium to initiate and sustain EMT. Moreover, *Loxl2* and *Fbln2* expression was reduced and *Ptx3* expression increased in the atrioventricular valves of E14.5 *Jag1^flox;Nkx2.5-Cre* mouse mutants, which show hyperplastic valves and defective remodeling (13). These gene expression changes paralleled those observed in the secretome and suggest that imbalanced ECM molecule expression may underlie impaired valve organization and remodeling.

We have thus identified three potential secretome markers by which NOTCH might contribute noncell autonomously to EMT: LOXL2, FBLN2, and PTX3. LOXL2 is a member of the lysyl oxidase family, which plays a major role in ECM remodeling through the crosslinking of collagens and elastin (57) and is involved in the posttranslational regulation of the EMT driver SNAIL (58). FBLN2 is a matrix glycoprotein that plays a central role in matrix stabilization, functioning as an intermolecular clasp and facilitating supra-molecular assembly of collagen IV, fibronectin, and other ECM molecules (59). In the heart, FBLN2 is produced by the endocardial cushion tissue (60) and has been suggested to maintain the mechanical properties of the heart valves (61). PTX3 is a member of the pentraxin family involved in the control of tumor development, affecting cell proliferation and EMT in human melanoma cells *in vitro* (49). hPTX3 overexpression causes the down-regulation of the early mesenchymal markers *SNAIL1* and *SNAIL2*, paralleled by *E-CADHERIN* up-regulation, indicating that PTX3 overexpression inhibits EMT in melanoma cells by reversing their mesenchyme phenotype to an epithelial one (49). Remarkably, PTX3 is the secreted factor that exhibited the most restricted localization to the cardiac cushions and valves.

In summary, our results validate MEEC as a powerful *in vitro* model for the study of the endocardial secretome. Manipulation of NOTCH signaling has revealed the DLL4- and JAG1-induced secretomes, and identified several secreted factors whose transcripts are expressed during cushion formation and valve remodeling and are altered in NOTCH mutant mice. Functional analysis of these factors will provide insight into how these signals are coordinated and how their disruption might contribute to congenital valve defects and disease.

DATA AVAILABILITY

The data set (raw files, protein databases, search parameters, and results) is available in the PeptideAtlas repository, which can be downloaded via http://www.peptideatlas.org/ with the dataset identifier PASS01354.

REFERENCES

1. Ma, L., Lu, M. F., Schwartz, R. J., and Martin, J. F. (2005) Bmp2 is essential for cardiac cushion epithelial-mesenchymal transition and myocardial patterning. *Development* **132,** 5601–5611

2. Rivera-Feliciano, J., and Tabin, C. J. (2006) Bmp2 instructs cardiac progenitors to form the heart-valve-inducing field. *Dev. Biol.* **295,** 580–588

3. Del Monte, G., Grego-Bessa, J., Gonzalez-Rajal, A., Bolos, V., and De La Pompa, J. L. (2007) Monitoring Notch1 activity in development: Evidence for a feedback regulatory loop. *Dev. Dyn.* **236,** 2594–2614

4. Luna-Zurita, L., Prados, B., Grego-Bessa, J., Luxán, G., del Monte, G., Benguría, A., Adams, R. H., Pérez-Pomares, J. M., and de la Pompa, J. L. (2010) Integration of a Notch-dependent mesenchymal gene program and Bmp2-driven cell invasiveness regulates murine cardiac valve formation. *J. Clin. Invest.* **120,** 3493–3507

5. Papoutsi, T., Luna-Zurita, L., Prados, B., Zaffran, S., and de la Pompa, J. L. (2018) Bmp2 and Notch cooperate to pattern the embryonic endocardium. *Development* **145,** pii

6. Hinton, R. B., and Yutzey, K. E. (2011) Heart valve structure and function in development and disease. *Annu. Rev. Physiol.* **73,** 29–46

7. Kopan, R., and Ilagan, M. X. (2009) The canonical Notch signaling pathway: Unfolding the activation mechanism. *Cell* **137,** 216–233

8. Rones, M. S., McLaughlin, K. A., Raffin, M., and Mercola, M. (2000) Serrate and Notch specify cell fates in the heart field by suppressing cardiomyogenesis. *Development* **127,** 3865–3876

9. MacGrogan, D., Munch, J., and de la Pompa, J. L. (2018) Notch and interacting signalling pathways in cardiac development, disease, and regeneration. *Nat. Rev. Cardiol.* **15,** 685–704

10. D'Amato, G., Luxán, G., del Monte-Nieto, G., Martínez-Poveda, B., Torroja, C., Walter, W., Bochter, M. S., Benedito, R., Cole, S., Martinez, F., Hadjantonakis, A.-K., Uemura, A., Jiménez-Borreguero, L. J., and de la Pompa, J. L. (2016) Sequential Notch activation regulates ventricular chamber development. *Nature Cell Biol.* **18,** 7–20

11. Grego-Bessa, J., Luna-Zurita, L., del Monte, G., Bolos, V., Melgar, P., Arandilla, A., Garratt, A. N., Zang, H., Mukouyama, Y. S., Chen, H., Shou, W., Ballestar, E., Esteller, M., Rojas, A., Perez-Pomares, J. M., and de la Pompa, J. L. (2007) Notch signaling is essential for ventricular chamber development. *Dev. Cell* **12,** 415–429

12. Luxán, G., Casanova, J. C., Martínez-Poveda, B., Prados, B., D'Amato, G., MacGrogan, D., Gonzalez-Rajal, A., Dobarro, D., Torroja, C., Martinez, F., Izquierdo-Garcia, J. L., Fernández-Friera, L., Sabater-Molina, M., Kong, Y. Y., Pizarro, G., Ibañez, B., Medrano, C., Garcia-Pavia, P., Gimeno, J. R., Monserrat, L., Jiménez-Borreguero, L. J., and de la Pompa, J. L. (2013) Mutations in the NOTCH pathway regulator MIB1 cause left ventricular noncompaction cardiomyopathy. *Nat. Med.* **19,** 193–201

13. MacGrogan, D., D'Amato, G., Travisano, S., Martinez-Poveda, B., Luxán, G., del Monte-Nieto, G., Papoutsi, T., Sbroggio, M., Bou, V., Gomez-del Arco, P., Gómez Manuel, J., Zhou, B., Redondo Juan, M., Jiménez-Borreguero Luis, J., and de la Pompa José, L. (2016) Sequential ligand-dependent Notch signaling activation regulates valve primordium formation and morphogenesis. *Circ. Res.* **118,** 1480–1497

14. Benedito, R., Roca, C., Sörensen, I., Adams, S., Gossler, A., Fruttiger, M., and Adams, R. H. (2009) The Notch Ligands Dll4 and Jagged1 Have Opposing Effects on Angiogenesis. *Cell* **137,** 1124–1135

15. Navarro, P., Trevisan-Herraz, M., Bonzon-Kulichenko, E., Nuñez, E., Martínez-Acedo, P., Perez-Hernández, D., Jorge, I., Mesa, R., Calvo, E., Carrascal, M., Hernáez, M. L., Garcia, F., Barcena, J. A., Ashman, K., Abian, J., Gil, C., Redondo, J. M., and Vázquez, J. (2014) General statistical framework for quantitative proteomics by stable isotope labeling. *J. Proteome Res.* **13,** 1234–1247

16. Martínez-Acedo, P., Nuñez, E., Gómez, F. J., Moreno, M., Ramos, E., Izquierdo-Álvarez, A., Miró-Casas, E., Mesa, R., Rodriguez, P., Martinez-Ruiz, A., Dorado, D. G., Lamas, S., and Vázquez, J. (2012) A novel strategy for global analysis of the dynamic thiol redox proteome. *Mol. Cell. Proteomics* **11,** 800–813

17. García-Marqués, F., Trevisan-Herraz, M., Martínez-Martínez, S., Camafeita, E., Jorge, I., Lopez, J. A., Méndez-Barbero, N., Méndez-Ferrer, S., Del Pozo, M. A., Ibáñez, B., Andrés, V., Sánchez-Madrid, F., Redondo, J. M., Bonzon-Kulichenko, E., and Vázquez, J. (2016) A novel systems-biology algorithm for the analysis of coordinated protein responses using quantitative proteomics. *Mol. Cell. Proteomics* **15,** 1740–1760

18. Trevisan-Herraz, M., Bagwan, N., Garcia-Marques, F., Rodriguez, J. M., Jorge, I., Ezkurdia, I., Bonzon-Kulichenko, E., and Vazquez, J. (2019) SanXoT: A modular and versatile package for the quantitative analysis of high-throughput proteomics experiments. *Bioinformatics* **35,** 1594–1596

19. Martínez-Bartolomé, S., Navarro, P., Martín-Maroto, F., López-Ferrer, D., Ramos-Fernández, A., Villar, M., García-Ruiz, J. P., and Vázquez, J. (2008) Properties of average score distributions of SEQUEST: The probability ratio method. *Mol. Cell. Proteomics* **7,** 1135–1145

20. Navarro, P., and Vázquez, J. (2009) A refined method to calculate false discovery rates for peptide identification using decoy databases. *J. Proteome Res.* **8,** 1792–1796

21. Bonzon-Kulichenko, E., Garcia-Marques, F., Trevisan-Herraz, M., and Vázquez, J. (2015) Revisiting peptide identification by high-accuracy mass spectrometry: Problems associated with the use of narrow mass precursor windows. *J. Proteome Res.* **14,** 700–710

22. Bonzon-Kulichenko, E., Martinez-Martinez, S., Trevisan-Herraz, M., Navarro, P., Redondo, J. M., and Vazquez, J. (2011) Quantitative in-depth analysis of the dynamic secretome of activated Jurkat T-cells. *J Proteomics* **75,** 561–571

23. Krogh, A., Larsson, B., von Heijne, G., and Sonnhammer, E. L. L. (2001) Predicting transmembrane protein topology with a hidden markov model: application to complete genomes11Edited by F. Cohen. *Journal of Molecular Biology* **305,** 567–580

24. Bendtsen, J. D., Jensen, L. J., Blom, N., Von Heijne, G., and Brunak, S. (2004) Feature-based prediction of non-classical and leaderless protein secretion. *Protein Eng. Des. Sel.* **17,** 349–356

25. Metsalu, T., and Vilo, J. (2015) ClustVis: A web tool for visualizing clustering of multivariate data using principal component analysis and heatmap. *Nucleic Acids Res.* **43,** W566–W570

26. Zambon, A. C., Gaj, S., Ho, I., Hanspers, K., Vranizan, K., Evelo, C. T., Conklin, B. R., Pico, A. R., and Salomonis, N. (2012) GO-Elite: A flexible solution for pathway and ontology over-representation. *Bioinformatics* **28,** 2209–2210

27. Szklarczyk, D., Franceschini, A., Wyder, S., Forslund, K., Heller, D., Huerta-Cepas, J., Simonovic, M., Roth, A., Santos, A., Tsafou, K. P., Kuhn, M., Bork, P., Jensen, L. J., and von Mering, C. (2015) STRING v10: Protein-protein interaction networks, integrated over the tree of life. *Nucleic Acids Res.* **43,** D447–D452

28. Shannon, P., Markiel, A., Ozier, O., Baliga, N. S., Wang, J. T., Ramage, D., Amin, N., Schwikowski, B., and Ideker, T. (2003) Cytoscape: A software environment for integrated models of biomolecular interaction networks. *Genome Res.* **13,** 2498–2504

29. Kanzler, B., Kuschert, S. J., Liu, Y. H., and Mallo, M. (1998) Hoxa-2 restricts the chondrogenic domain and inhibits bone formation during development of the branchial area. *Development* **125,** 2587–2597

30. Pompa de la, JL, Wakeham, A., Correia, K. M., Samper, E., Brown, S., Aguilera, R. J., Nakano, T., Honjo, T., Mak, T. W., Rossant, J., and Conlon, R. A. (1997) Conservation of the Notch signalling pathway in mammalian neurogenesis. *Development* **124,** 1139–1148

31. Kisanuki, Y. Y., Hammer, R. E., Miyazaki, J. Williams, S. C., Richardson, J. A., and Yanagisawa, M. (2001) Tie2-Cre transgenic mice: A new model for endothelial cell-lineage analysis in vivo. *Dev.l Biol.* **230,** 230–242

32. Stanley, E. G., Biben, C., Elefanty, A., Barnett, L., Koentgen, F., Robb, L., and Harvey, R. P. (2002) Efficient Cre-mediated deletion in cardiac progenitor cells conferred by a 3′UTR-ires-Cre allele of the homeobox gene Nkx2–5. *Int. J. Dev. Biol.* **46,** 431–439

33. Koch, U., Fiorini, E., Benedito, R., Besseyrias, V., Schuster-Gossler, K., Pierres, M., Manley, N. R., Duarte, A., Macdonald, H. R., and Radtke, F. (2008) Delta-like 4 is the essential, nonredundant ligand for Notch1 during thymic T cell lineage commitment. *J. Exp. Med.* **205,** 2515–2523

34. Mancini, S. J., Mantei, N., Dumortier, A., Suter, U., MacDonald, H. R., and Radtke, F. (2005) Jagged1-dependent Notch signaling is dispensable for hematopoietic stem cell self-renewal and differentiation. *Blood* **105,** 2340–2342

35. Wurmser, A. E., Nakashima, K., Summers, R. G., Toni, N., D'Amour, K. A., Lie, D. C., and Gage, F. H. (2004) Cell fusion-independent differentiation of neural stem cells to the endothelial lineage. *Nature* **430,** 350–356

36. McLaughlin, F., Ludbrook, V. J., Kola, I., Campbell, C. J., and Randi, A. M. (1999) Characterisation of the tumour necrosis factor (TNF)-(alpha) response elements in the human ICAM-2 promoter. *J. Cell Sci.* **112,** 4695–4703

37. Clipstone, N. A., and Crabtree, G. R. (1992) Identification of calcineurin as a key signalling enzyme in T-lymphocyte activation. *Nature* **357,** 695–697

38. DeCicco-Skinner, K. L., Henry, G. H., Cataisson, C., Tabib, T., Gwilliam, J. C., Watson, N. J., Bullwinkle, E. M., Falkenburg, L., O'Neill, R. C., Morin, A., and Wiest, J. S. (2014) Endothelial cell tube formation assay for the in vitro study of angiogenesis. *J. Vis. Exp.* **91,** e51312

39. Lamar, E., Deblandre, G., Wettstein, D., Gawantka, V., Pollet, N., Niehrs, C., and Kintner, C. (2001) Nrarp is a novel intracellular component of the Notch signaling pathway. *Genes Dev.* **15,** 1885–1899

40. Iso, T., Kedes, L., and Hamamori, Y. (2003) HES and HERP families: Multiple effectors of the notch signaling pathway. *J. Cell. Physiol.* **194,** 237–255

41. Fischer, A., Schumacher, N., Maier, M., Sendtner, M., and Gessler, M. (2004) The Notch target genes Hey1 and Hey2 are required for embryonic vascular development. *Genes Dev.* **18,** 901–911

42. Vanlandingham, P. A., and Ceresa, B. P. (2009) Rab7 regulates late endocytic trafficking downstream of multivesicular body biogenesis and cargo sequestration. *J. Biol. Chem.* **284,** 12110–12124

43. Timmerman, L. A., Grego-Bessa, J., Raya, A., Bertrán, E., Pérez-Pomares, J. M., Díez, J., Aranda, S., Palomo, S., McCormick, F., Izpisúa-Belmonte, J. C., and de la Pompa, J. L. (2004) Notch promotes epithelial-mesenchymal transition during cardiac development and oncogenic transformation. *Genes Dev.* **18,** 99–115

44. Jain, R., Engleka, K. A., Rentschler, S. L., Manderfield, L. J., Li, L., Yuan, L., and Epstein, J. A. (2011) Cardiac neural crest orchestrates remodeling and functional maturation of mouse semilunar valves. *J. Clin. Invest.* **121,** 422–430

45. Jain, R., Rentschler, S., and Epstein, J. A. (2010) Notch and cardiac outflow tract development. *Ann. N.Y. Acad. Sci.* **1188,** 184–190

46. Potts, J. D., and Runyan, R. B. (1989) Epithelial-mesenchymal cell transformation in the embryonic heart can be mediated, in part, by transforming growth factor β. *Dev. Biol.* **134,** 392–401

47. Boyer, A. S., Ayerinskas, I. I., Vincent, E. B., McKinney, L. A., Weeks, D. L., and Runyan, R. B. (1999) TGFβ2 and TGFβ3 have separate and sequential activities during epithelial–mesenchymal cell transformation in the embryonic heart. *Dev. Biol.* **208,** 530–545

48. Moon, H.-J., Finney, J., Ronnebaum, T., and Mure, M. (2014) Human lysyl oxidase-like 2. *Bioorganic Chem.* **57,** 231–241

49. Ronca, R., Di Salle, E., Giacomini, A., Leali, D., Alessi, P., Coltrini, D., Ravelli, C., Matarazzo, S., Ribatti, D., Vermi, W., and Presta, M. (2013) Long pentraxin-3 inhibits epithelial–mesenchymal transition in melanoma cells. *Mol. Cancer Therap.* **12,** 2760–2771

50. Qureshi, H. Y., Sylvester, J., El Mabrouk, M., and Zafarullah, M. (2005) TGF-β-induced expression of tissue inhibitor of metalloproteinases-3 gene in chondrocytes is mediated by extracellular signal-regulated kinase pathway and Sp1 transcription factor. *J. Cell. Physiol.* **203,** 345–352

51. de Vega, S., Iwamoto, T., and Yamada, Y. (2009) Fibulins: Multiple roles in matrix structures and tissue functions. *Cell. Mol. Life Sci.* **66,** 1890–1902

52. Horiguchi, M., Ota, M., and Rifkin, D. B. (2012) Matrix control of transforming growth factor-β function. *J. Biochem.* **152,** 321–329

53. del Monte-Nieto, G., Ramialison, M., Adam, A. A. S., Wu, B., Aharonov, A., D'Uva, G., Bourke, L. M., Pitulescu, M. E., Chen, H., de la Pompa, J. L., Shou, W., Adams, R. H., Harten, S. K., Tzahor, E., Zhou, B., and Harvey, R. P. (2018) Control of cardiac jelly dynamics by NOTCH1 and NRG1 defines the building plan for trabeculation. *Nature* **557,** 439–445

54. Epstein, J. A., Aghajanian, H., and Singh, M., K. (2015) Semaphorin signaling in cardiovascular development. *Cell Metabolism* **21,** 163–173

55. Azhar, M., Runyan, R. B., Gard, C., Sanford, L. P., Miller, M. L., Andringa, A., Pawlowski, S., Rajan, S., and Doetschman, T. (2009) Ligand-specific function of transforming growth factor beta in epithelial-mesenchymal transition in heart development. *Dev. Dyn.* **238,** 431–442

56. Dickson, M. C., Slager, H. G., Duffie, E., Mummery, C. L., and Akhurst, R. J. (1993) RNA and protein localisations of TGF beta 2 in the early mouse embryo suggest an involvement in cardiac development. *Development* **117,** 625–639

57. Kim, Y.-M., Kim, E.-C., and Kim, Y. (2011) The human lysyl oxidase-like 2 protein functions as an amine oxidase toward collagen and elastin. *Mol. Biol. Rep.* **38,** 145–149

58. Peinado, H., Del Carmen Iglesias-de la Cruz, M., Olmeda, D., Csiszar, K., Fong, K. S. K., Vega, S., Nieto, M. A., Cano, A., and Portillo, F. (2005) A molecular role for lysyl oxidase-like 2 enzyme in snail regulation and tumor progression. *EMBO J.* **24,** 3446–3458

59. Baird, B. N., Schliekelman, M. J., Ahn, Y.-H., Chen, Y., Roybal, J. D., Gill, B. J., Mishra, D. K., Erez, B., O'Reilly, M., Yang, Y., Patel, M., Liu, X., Thilaganathan, N., Larina, I. V., Dickinson, M. E., West, J. L., Gibbons, D. L., Liu, D. D., Kim, M. P., Hicks, J. M., Wistuba, I. I., Hanash, S. M., and Kurie, J. M. (2013) Fibulin-2 is a driver of malignant progression in lung adenocarcinoma. *PloS One* **8,** e67054

60. Zhang, H.-Y., Chu, M.-L., Pan, T.-C., Sasaki, T., Timpl, R., and Ekblom, P. (1995) Extracellular matrix protein fibulin-2 is expressed in the embryonic endocardial cushion tissue and is a prominent component of valves in adult heart. *Dev. Biol.* **167,** 18–26

61. Tsuda, T., Wang, H., Timpl, R., and Chu, M.-L. (2001) Fibulin-2 expression marks transformed mesenchymal cells in developing cardiac valves, aortic arch vessels, and coronary vessels. *Dev. Dyn.* **222,** 89–100